

The kinematics of cluster galaxies via velocity dispersion profiles

Lawrence E. Bilton[★] and Kevin A. Pimblet

E.A. Milne Centre for Astrophysics, The University of Hull, Cottingham Road, Kingston upon Hull HU6 7RX, UK

Accepted 2018 August 29. Received 2018 August 29; in original form 2017 December 1

ABSTRACT

We present an analysis of the kinematics of a sample of 14 galaxy clusters via velocity dispersion profiles (VDPs), compiled using cluster parameters defined within the X-Ray Galaxy Clusters Database (BAX) cross-matched with data from the Sloan Digital Sky Survey (SDSS). We determine the presence of substructure in the clusters from the sample as a proxy for recent core mergers, resulting in 4 merging and 10 non-merging clusters to allow for comparison between their respective dynamical states. We create VDPs for our samples and divide them by mass, colour, and morphology to assess how their kinematics respond to the environment. To improve the signal-to-noise ratio our galaxy clusters are normalized and co-added to a projected cluster radius at 0.0–2.5 r_{200} . We find merging cluster environments possess an abundance of a kinematically active (rising VDP) mix of red and blue elliptical galaxies, which is indicative of infalling substructures responsible for pre-processing galaxies. Comparatively, in non-merging cluster environments galaxies generally decline in kinematic activity as a function of increasing radius, with bluer galaxies possessing the highest velocities, likely as a result of fast infalling field galaxies. However, the variance in kinematic activity between blue and red cluster galaxies across merging and non-merging cluster environments suggests galaxies exhibit differing modes of galaxy accretion on to a cluster potential as a function of the presence of a core merger.

Key words: galaxies: clusters: general – galaxies: kinematics and dynamics.

1 INTRODUCTION

Galaxies are known to follow a morphology–density relation, which is pronounced in clusters of galaxies (Oemler 1974; Dressler 1980; Smith et al. 2005). Late-type galaxies are found to dominate at large radii from a galaxy cluster centre, predominantly within the field population. Conversely, early-type galaxies are found to pervade the denser regions at smaller radii, well within galaxy clusters. There are further observable environmental side effects that follow similar patterns, such as the apparent bimodality of the colour–density relation (Hogg et al. 2003, 2004), where denser regions are populated with quenched, red and elliptical galaxies. Contrarily star-forming, blue and spiral morphologies are found out towards the field population (e.g. Lewis et al. 2002; Gómez et al. 2003; Bamford et al. 2009).

Galaxy clusters are consequently an epicentre for environmental interactions. The comparative accretion histories of cluster galaxies between galaxy clusters and the field population can be determined as a function of their environment, indicated by their membership’s morphology, colour, and star formation assuming a fixed stellar mass (e.g. Postman & Geller 1984; Hogg et al. 2004; von der Linden et al. 2010). The evolutionary transformation of cluster galaxies

could have transpired prior to a galaxy’s accretion on to a cluster’s potential, since the field population’s morphologies, colours, and rate of star formation are mixed (e.g. Kauffmann et al. 2004; Blanton et al. 2005). Or, it is possible that the harassment and accretion of a galaxy by a cluster leads on to a transformation of blue to red; star forming to non-star forming; spiral to elliptical (Moore et al. 1996). This metamorphosis during the infall of a galaxy into a cluster is considered to be the result of an increased probability of tidal galaxy–galaxy interaction mechanisms, or, even the tidal field of the cluster itself. The former being more likely to give rise to the stripping of material, and distortion of a galaxy’s structure (Moore et al. 1999). Further observations ostensibly show the shifting of morphologies from late-type to early-type is chiefly the result of mergers between two galaxies (e.g. Owers et al. 2012).

The volume between cluster galaxies contains a sea of hot diffuse gas that represents an intracluster medium (ICM), another form of environmental interaction. An infalling galaxy approaching a cluster centre at higher velocities relative to the ICM will experience ram-pressure stripping (Gunn & Gott 1972; Abadi, Moore & Bower 1999; Quilis, Moore & Bower 2000; Sheen et al. 2017). The disc of cold gas surrounding an infalling galaxy will be stripped away over small time-scales, however, as the ICM density increases during infall so do the time-scales of this process (Roediger & Brüggen 2007). The result of this process retards rates of star formation to where the infalling galaxy will be quenched completely. The diffuse nature

[★] E-mail: l.bilton@2016.hull.ac.uk

of any hot gas haloes surrounding infalling galaxies lends to their increased likelihood of being ejected from the galaxy’s potential. Therefore, the removal of any surrounding haloes of hot gas around an infalling galaxy will inhibit the replenishment of their cold gas reservoirs through radiative cooling, slowly strangling galaxy star formation, with any remaining cold gas being exhausted (Larson, Tinsley & Caldwell 1980). Ram-pressure stripping has been found to be prevalent in the dense cores of clusters through observations of tails with H I and H α emission lines that are associated with a parent galaxy (e.g. Gavazzi et al. 2001; Cortese et al. 2007).

With galaxy cluster environments hosting extended ICM haloes that interact significantly with field and infalling galaxies, consideration of a cluster’s size is therefore needed in order to understand where the boundary between these environments lies. One common definition of a cluster’s size is the virial radius, commonly approximated as $R_{\text{vir}} \sim r_{200}$. r_{200} represents the radial point at which the average density is ~ 200 times the critical density (e.g. von der Linden et al. 2010; Pimblet & Jensen 2012; Bahé et al. 2013; Pimblet, Penny & Davies 2014). However, the proposed splashback radius may represent a more physical boundary, extending farther than r_{200} (e.g. More, Diemer & Kravtsov 2015; More et al. 2016; Baxter et al. 2017). The splashback radius represents the first apoapsis of an observed accreted galaxy that has already passed through its first periapsis or turnaround (Sanchis et al. 2004; Pimblet et al. 2006). Despite both of these definitions for a potential cluster boundary, they do not extend to the radii observed with harassed galaxies infalling to the cluster centre; colour densities and effects on star formation can continue beyond these defined boundaries (e.g. Balogh et al. 1999; Haines et al. 2009; von der Linden et al. 2010; Haines et al. 2015). A plethora of observations and simulations appear to indicate that there is a natural fluidity between the local cluster environment and the field population of late-type star-forming galaxies. Such simulations have shown the entire cluster boundary to expand even grander scales with ICM haloes extending out to radii of ~ 10 Mpc from the cluster centre (Frenk et al. 1999).

The existence of these large-scale structures therefore indicates the presence of smaller scale clumping of galaxies; more layers of substructure within galaxy clusters are expected (Dressler & Shectman 1988). It is more likely that any accreted galaxies from the field population will undergo ‘pre-processing’ into smaller galaxy groups that help form the substructure within a cluster (e.g. Berrier et al. 2009; Bahé et al. 2013), inducing evolutionary changes prior to traditional cluster galaxy infall and accretion. In the simulation work of Haines et al. (2015) it is found that star-forming galaxies are unexpectedly quenched at large radii from the cluster centre, models can only account for this if the galaxies have undergone pre-processing into a substructure prior to any further interaction. There is an alternative variant of pre-processing in rarer cluster–cluster merger events, the most famous example of such an event is the Bullet Cluster (Tucker et al. 1998). X-ray observations of the Bullet Cluster show a smaller subcluster of galaxies colliding with a larger cluster, thereby ram-pressure stripping causing the removal of the surrounding hot gas (Markevitch et al. 2002). Other ‘bullet-like’ events are shown to affect the local galactic environment in equivalent ways (e.g. Owers et al. 2011; Owers et al. 2012).

This leads on to potential ways to make a comparison between these different environments via their varying dynamical states. We can therefore probe the variation in cluster environments via analysis of the cluster kinematics as a function of radius with velocity dispersion profiles (VDPs). VDPs represent how the radial velocity dispersions vary from the dense area of accreted early-type galaxies within r_{200} , out to sparser star-forming late-types on

their infall journey to the centre (see Hou et al. 2009, 2012). It is therefore possible to test how the shape of a VDP is affected by binning a profile based on different cluster galaxy properties. As an example, Pimblet & Jensen (2012) split the VDP of Abell 1691 into individual high- and low-mass profiles. It is found that there is a large disparity in the velocities between the high- and low-mass samples; Pimblet & Jensen (2012) argue the large high-mass sample velocities could be due to the presence of substructure, or recent arrivals to the system. The shape of the VDP could, however, be affected by any evolutionary change due to the cluster environment.

In this work, we aim to test how the average cluster VDP’s shape can be altered as a function of radius, parametrized by its member’s different evolutionary stages through proxies of varying masses, colours, and morphologies, in order to explore the varying dynamics between merging, dynamically active, and non-merging, relaxed environments. We therefore present galaxy data taken from the Sloan Digital Sky Survey (SDSS) to form a membership from a defined cluster sample determined from an X-ray catalogue. Details on how the data were acquired can be found in Section 2. Details on the derivation and production of the VDPs can be found in Section 3. A discussion of the data, results, and their consequences are outlined in Section 4, followed by a summary of our conclusions in Section 5.

Throughout the work presented here, we assume a Λ CDM model of cosmology with $\Omega_M = 0.3$, $\Omega_\Lambda = 0.7$, and $H_0 = 100h$ km s $^{-1}$ Mpc $^{-1}$, where $h = 0.7$.

2 THE DATA

We define a sample of galaxy clusters using the X-Ray Galaxy Clusters Database (BAX; Sadat et al. 2004), a comprehensive catalogue of X-ray emitting clusters from multiple literary sources. For each galaxy cluster, we obtain members from SDSS Data Release 8 (DR8; Aihara et al. 2011) with complementary data from MPA-JHU Value Added Catalogue (Kauffmann et al. 2003; Brinchmann et al. 2004; Tremonti et al. 2004). We use data from Galaxy Zoo 2 (GZ2; Willett et al. 2013; Hart et al. 2016) to provide morphological information on member galaxies.

2.1 Defining the cluster sample and their membership

To select our cluster sample, we adopt an X-ray luminosity range of $3 < L_X < 30 \times 10^{44}$ erg s $^{-1}$. These limits ensure we are selecting the most massive clusters from the BAX catalogue across a range of dynamically relaxed and perturbed states. We impose a redshift range of $0.0 < z < 0.1$, which serves to help make the final sample of galaxies making each cluster complete. The imposed limits with BAX output a base sample size of 68 clusters.

For each of the clusters in the sample a 10 Mpc h^{-1} upper radial limit of DR8 galaxies is applied from the BAX defined centre to the appropriate scales, using the flat cosmology prescribed in Section 1 (Wright 2006). All candidate clusters have their global means (\bar{c}_{glob}) and velocity dispersions (σ_{glob}) calculated for galaxies ≤ 1.5 Mpc h^{-1} ; the latter are determined by the square root of the biweight mid-variance (see Beers, Flynn & Gebhardt 1990). Due to a willingness to observe the effect infall galaxies have on VDPs beyond r_{200} , a constant line boundary applied in velocity space is not ideal to distinguish an infaller from the field, since a cluster’s potential varies with increasing R from the centre. Using the mass estimation method of caustics (Diaferio & Geller 1997; Diaferio 1999), we produce surface caustics with velocity limits

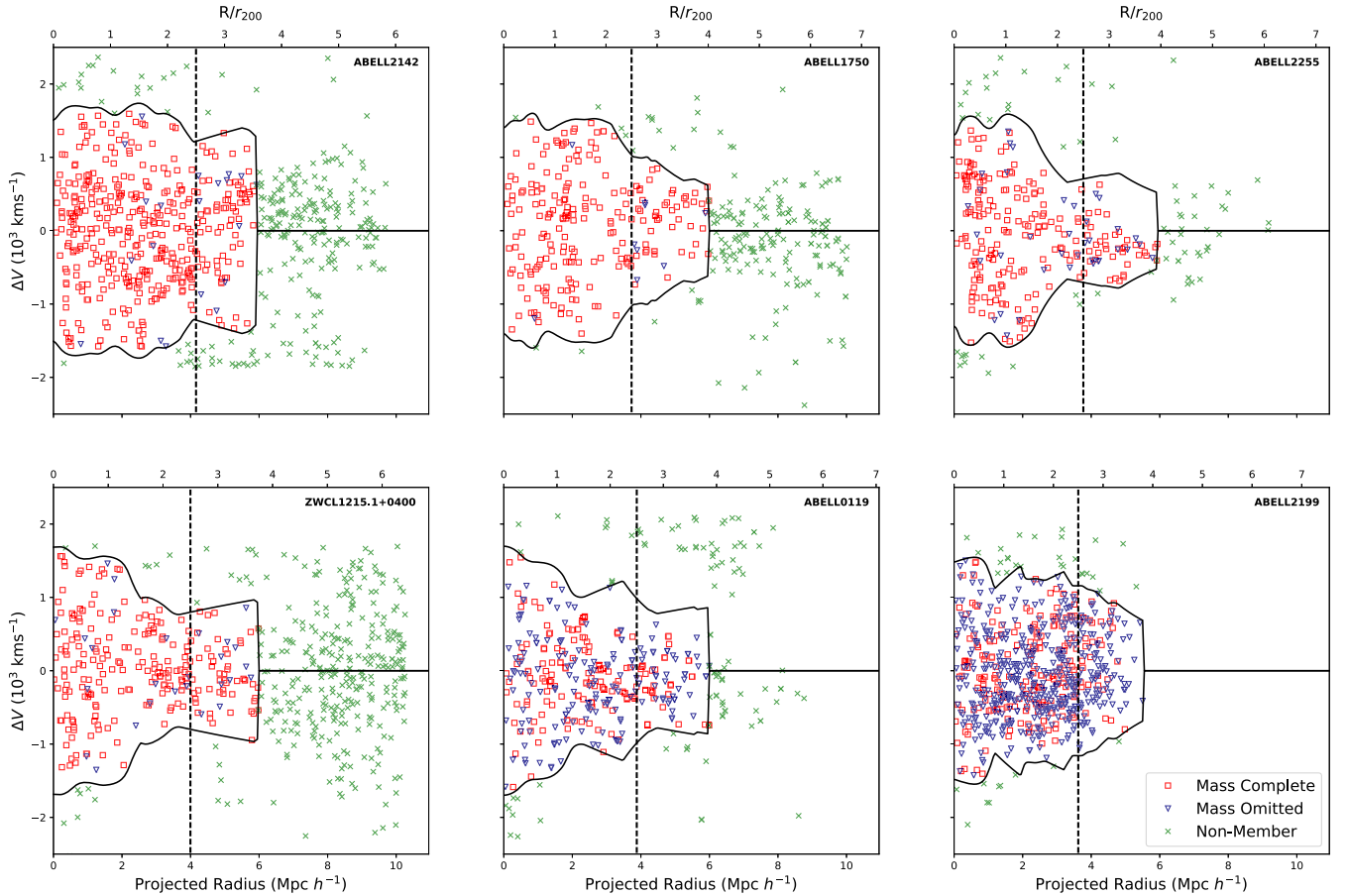


Figure 1. A selection of example surface caustics (the black curves) from the final merging cluster sample (top row) and non-merging cluster sample (bottom row). Where the red squares represent the galaxies that make a complete sample at $\log_{10}(M_*) \geq 10.1$, with the blue triangles representing omitted galaxies that are at $\log_{10}(M_*) < 10.1$. Galaxies that lie within the surface caustics are considered to be cluster members. Here the radial velocity (ΔV) with respect to the cluster’s mean recession velocity is plotted against the projected radius in units of $\text{Mpc } h^{-1}$ and R/r_{200} . The black dashed vertical lines represent the $2.5 R/r_{200}$ radial cut of each cluster. Only galaxies of $\leq 2.5 R/r_{200}$ within the caustics are used in the production of the stacked VDPs.

of $\Delta V = \pm 1500 \text{ km s}^{-1}$ and a radial limit of $R \leq 10 \text{ Mpc } h^{-1}$, where $\Delta V = c[(z_{\text{gal}} - z_{\text{clu}})/(1 + z_{\text{clu}})]$. The surface caustics help determine the final membership that considers the varying potential as a function of R (Gifford & Miller 2013; Gifford, Miller & Kern 2013). The resultant caustic mass profiles allow for an estimation of r_{200} with the application of a varying enclosed density profile, $\rho(r) = 3M(r)/4\pi r^3$, until $\rho(r) = 200\rho_c$, where ρ_c is the critical density of the Universe for our flat cosmology. An example of these surface caustics is shown in Fig. 1 and is discussed in Section 4.2.

The final values for σ_{glob} , $\sigma_{r_{200}}$ for galaxies $\leq r_{200}$ and $\overline{c\bar{z}}_{\text{glob}}$ are determined. The uncertainties for these parameters are calculated following the methodology of Danese, de Zotti & di Tullio (1980). In order to maximize the number of DR8 galaxies per cluster while maintaining a mass-complete sample across our redshift range, we impose a stellar mass limit of $\log_{10}(M_*) \geq 10.1$. Candidate clusters are then cross-checked with the Einasto et al. (2001) catalogue of superclusters to help eliminate those structures that overlap with one another. A final check we employ before a cluster is added to the final master sample is to test if the cluster is sufficiently rich in its membership of cluster galaxies. We define the richness limit here as clusters with > 50 galaxies at $\leq r_{200}$, any clusters not meeting this requirement are ignored. This leads to a resultant sample size of 14 galaxy clusters.

2.2 Merging cluster sample

For the thesis of this work, we create subset samples of merging and non-merging galaxy cluster systems in order to compare how their respective environments affect the kinematics of their members. To determine whether or not a cluster is merging we employ the Δ test of substructure devised by Dressler & Shectman (1988) on galaxies $\leq 1.5 \text{ Mpc } h^{-1}$ from the BAX defined cluster centre. The Δ test methodology takes the local mean radial velocity ($\overline{c\bar{z}}_{\text{local}}$) and local standard deviation of the radial velocity (σ_{local}) of a galaxy and its $N_{\text{nn}} = \sqrt{N_{\text{glob}}}$ nearest neighbours, where N_{glob} is the number of galaxies $< 1.5 \text{ Mpc } h^{-1}$. These are then compared to the global values of the cluster they are the members of, as shown in equation (1).

$$\delta_i^2 = \left(\frac{N_{\text{nn}} + 1}{\sigma_{\text{glob}}^2} \right) [(\overline{c\bar{z}}_{\text{local}} - \overline{c\bar{z}}_{\text{glob}})^2 + (\sigma_{\text{local}} - \sigma_{\text{glob}})^2], \quad (1)$$

where δ measures the deviation in the small region around the galaxy compared to the global cluster values at $\leq 1.5 \text{ Mpc } h^{-1}$. This process is iterated through each galaxy to produce the sum $\Delta = \sum_i \delta_i$. Pinkney et al. (1996) have shown the Δ test to be the most sensitive for indicating the presence of substructure, demonstrating a ≥ 99 per cent significance in determining its occupancy. Therefore, a cluster will be classified as merging when substructure is detected

Table 1. The mass-complete merging cluster subset sample. The J2000 coordinates and X-ray luminosity values are taken from BAX. σ_{r200} is determined from a biweight estimator, as noted by Beers et al. (1990). The uncertainties for the mean recession velocities and velocity dispersions are calculated following the method by Danese et al. (1980). The σ_{ref} values are reference velocity dispersions from the literature. The $P(\Delta)$ values testing for substructure follow the methods of Dressler & Shectman (1988) with equation (1), those values that are $\ll 0.01$ strongly reject the null hypothesis and have values smaller than to three decimal places.

Name	RA (J2000)	Dec. (J2000)	L_x ($\times 10^{44}$ erg s $^{-1}$)	N_{r200}	$\overline{cz}_{\text{glob}}$ (km s $^{-1}$)	σ_{r200} (km s $^{-1}$)	σ_{ref} (km s $^{-1}$)	$P(\Delta)$
Abell 426	03 19 47.20	+41 30 47	15.34 ^a	97	5155 \pm 59	827 ⁺⁴⁰ ₋₄₇	1324 ¹	0.010
Abell 1750	13 30 49.94	-01 52 22	5.98 ^b	72	25 614 \pm 92	782 ⁺⁵⁶ ₋₇₂	657 ²	$\ll 0.01$
Abell 2142	15 58 20.00	+27 14 00	21.24 ^a	132	26 882 \pm 84	816 ⁺⁵² ₋₆₃	1193 ⁸	0.005
Abell 2255	17 12 31.05	+64 05 33	5.54 ^a	72	24 075 \pm 98	788 ⁺⁶⁰ ₋₇₉	1009 ⁴	$\ll 0.01$

Note. ¹ Struble & Rood (1999) ^a Reiprich & Böhringer (2002)

² Einasto et al. (2012) ^b Popesso et al. (2007)

³ Pearson, Batiste & Batuski (2014) ^c Böhringer et al. (2000)

⁴ Akamatsu et al. (2017)

Table 2. The mass-complete non-merging cluster subset sample is presented here, noting the null hypothesis is accepted where $P(\Delta) \geq 0.01$. All values and uncertainties are obtained and determined as detailed in Table 1.

Name	RA (J2000)	Dec. (J2000)	L_x ($\times 10^{44}$ erg s $^{-1}$)	N_{r200}	$\overline{cz}_{\text{glob}}$ (km s $^{-1}$)	σ_{r200} (km s $^{-1}$)	σ_{ref} (km s $^{-1}$)	$P(\Delta)$
Abell 85	00 41 37.81	-09 20 33	9.41 ^a	70	16 709 \pm 71	719 ⁺⁴⁵ ₋₅₅	979 ⁵	0.853
Abell 119	00 56 21.37	-01 15 46	3.30 ^a	59	13 279 \pm 74	752 ⁺⁴⁷ ₋₅₉	619 ⁶	0.579
Abell 1650	12 58 46.20	-01 45 11	6.99 ^a	50	25 087 \pm 98	671 ⁺⁵⁸ ₋₇₈	498 ²	0.636
Abell 1656	12 59 48.73	+27 58 50	7.77 ^a	145	6995 \pm 39	798 ⁺²⁷ ₋₂₉	973 ⁷	0.087
Abell 1795	13 49 00.52	+26 35 06	10.26 ^a	70	18 754 \pm 87	794 ⁺⁵⁶ ₋₆₉	662 ²	0.265
Abell 2029	15 10 58.70	+05 45 42	17.44 ^a	127	23 382 \pm 103	932 ⁺⁶³ ₋₇₉	973 ⁷	0.415
Abell 2061	15 21 15.31	+30 39 16	4.85 ^d	90	23 311 \pm 69	719 ⁺⁴³ ₋₅₃	898 ³	0.183
Abell 2065	15 22 42.60	+27 43 21	5.55 ^a	93	21 565 \pm 92	882 ⁺⁵⁷ ₋₇₂	1286 ³	0.211
Abell 2199	16 28 38.50	+39 33 60	4.09 ^a	67	9161 \pm 55	737 ⁺³⁶ ₋₄₂	722 ⁶	0.586
ZWCL1215	12 17 41.44	+03 39 32	5.17 ^a	97	23 199 \pm 98	671 ⁺⁵⁸ ₋₇₈	889 ⁹	0.873

Note. ² Einasto et al. (2012) ^a Reiprich & Böhringer (2002)

³ Pearson et al. (2014) ^d Marini et al. (2004)

⁵ Agulli et al. (2016)

⁶ Rines et al. (2003)

⁷ Sohn et al. (2017)

⁸ Munari, Biviano & Mamon (2014)

⁹ Zhang et al. (2011)

at $P(\Delta) \leq 0.01$. All clusters that reject the null hypothesis are added to the subset merging cluster sample. We discuss some of the caveats of this approach in Section 4.4. The resultant merging subset sample contains 4 galaxy clusters, detailed in Table 1, leaving the non-merging subset outweighing the mergers with 10 galaxy clusters, detailed in Table 2. Example bubble plots of merging and non-merging clusters from both samples are shown in Fig. 2, where the area of each circle is proportional to e^{δ_i} , indicating the level of substructuring through the magnitude of deviations from the global values.

3 VELOCITY DISPERSION PROFILES

The kinematics of each cluster within the sample are analysed from their respective VDPs, denoted as $\sigma_p(R)$. These VDPs can depict, with reasonable clarity, how dynamically complex or simple a cluster is. In this work we derive the VDPs computationally from the method prescribed by Bergond et al. (2006) for globular clusters. This has since been adapted to galaxy groups and clusters by Hou et al. (2009, 2012). The VDPs are produced from bins of the radial

velocities through a Gaussian window function that is weighted exponentially as a function of radius across all radii. However, in line with Harris (private communication), we note here the presence of a typographical error in the original notation of this function by Bergond et al. (2006), in which the exponential component should be denoted as negative rather than positive. This error appears to have been perpetuated into further works cited here (e.g. Hou et al. 2009; Hou et al. 2012; Pimblet et al. 2014). We therefore present the corrected version of this window function in equation (2), which can be seen in the body of the work by Woodley et al. (2007) under equation (3). The correct window function is written as

$$\omega_i = \frac{1}{\sigma_R} \exp\left[-\frac{(R - R_i)^2}{2\sigma_R^2}\right], \quad (2)$$

where the kernel width σ_R determines the size of a window that the radial velocities are binned against with the square-difference in radius $(R - R_i)^2$. The window is chosen to be $0.2R_{\text{max}}$ in units of r_{200} . This is to avoid the window being too large, thereby smoothing out features in the profile, or too small where spurious shapes in the profile could be produced by outliers. The window function ω_i is

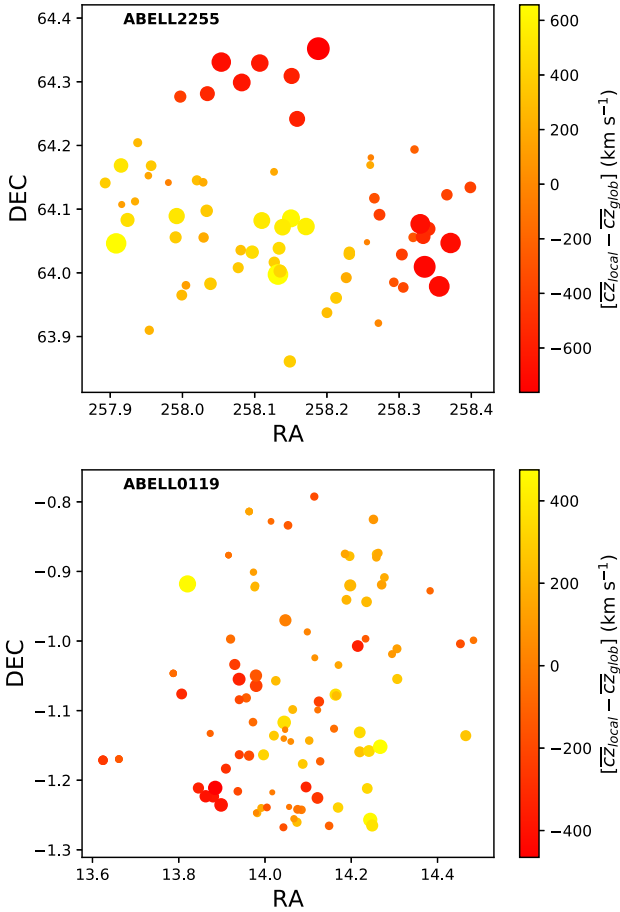


Figure 2. Example bubble plots from the Δ test, where the total area of each circle is proportional to the deviation e^{δ_i} , and the colours representing varying radial velocity differences $[\bar{c}_{z_{\text{local}}} - \bar{c}_{z_{\text{glob}}}]$. Cluster Abell 2255 (top) shows significant subclustering with a greater number of substantial deviations from the global values, as demonstrated by the overlapping larger area circles with large radial velocities. Cluster Abell 0119 (bottom) in comparison demonstrates weak subclustering, with fewer numbers of significantly strong deviations from the global values.

then applied to the projected VDP, which is written as

$$\sigma_P(R) = \sqrt{\frac{\sum_i \omega_i(R)(x_i - \bar{x})^2}{\sum_i \omega_i(R)}}, \quad (3)$$

where x_i represents the radial velocity of each galaxy inputted taken as a difference from \bar{x} , which represents the mean recession velocity of the cluster.

The inputted cluster data ideally should not have fewer than 20 galaxy members; this is to ensure the resultant projected VDPs are not spurious (Hou et al. 2009). This can potentially pose problems for wanting to observe the dynamics of a cluster based on varying galactic parameters due to the inadvertent biasing to smaller bin sizes. Applying the cluster richness criterion of 50 galaxy members at $\leq r_{200}$ provides an adequate safeguard against this problem while determining cluster membership. An example of the full non-split VDPs from each subsample is presented in Fig. 3. From this we can see the bins that reside within $1.5 \text{ Mpc } h^{-1}$ marry closely with the results from the Δ test for substructure, however, this is not found to be consistent across the entire sample of determined merging and non-merging systems. A problem that was noted by Pimblet et al. (2014), and could reflect the homogenization of certain clus-

ters where the weighting of the Gaussian moving window function causes a rise in response to more significant groupings of galaxies at larger radii.

In order to address the aims of this work, we compare the cluster environments between merging and non-merging systems with the kinematics of their member cluster galaxies through varying limits of different intrinsic cluster galaxy parameters. We therefore compute a series of VDPs with equations (2) and (3) outlined in Section 3 using the following methodology: Cluster galaxies are split between specific limits of varying galaxy properties of mass, morphology, and colour. These splits are passed through each cluster from both samples, with each cluster galaxy co-added to a normalized fixed grid of line-of-sight velocity ΔV , and projected radius R between 0 and $2.5 r_{200}$. Resulting in a stack for each of the merging and non-merging samples. Stacking for each subsample allows for a general picture of each environment to be built, to ascertain how the kinematics of differing subpopulations of galaxies within each environment are affected.

3.1 Mass

Analysis of varying stellar mass limits allows for basic inference of how differing galaxy populations may vary depending on its environment at incremental radii from its centre. Fixed limits are chosen for three profiles of different masses: $\log_{10}(M_*) \geq 10.8$, $10.5 \leq \log_{10}(M_*) < 10.8$, and $\log_{10}(M_*) < 10.5$. These limits are selected arbitrarily in order to maintain parity between the bin sizes of each range.

Fig. 4 shows the resultant stacks of the merging, and non-merging, clusters split via different stellar masses present in the DR8 data. In the merging stack, there is a prominent illustration of a dynamic environment, especially between the $\log_{10}(M_*) < 10.5$ and $\log_{10}(M_*) \geq 10.8$ profiles. The $\log_{10}(M_*) \geq 10.8$ mass profile shows a steadily increasing profile having the highest dispersion of velocities at $\sim 1.5 r_{200}$, in tandem with the $\log_{10}(M_*) < 10.5$ profile. The former commonly denoted as members of an accreted older population of galaxies, with the latter commonly associated with an accreted younger population. The $\log_{10}(M_*) \geq 10.8$ profile represents an increasing intensity of interacting, or merging, galaxies at $\lesssim 1.5 r_{200}$. The same can be determined with the $\log_{10}(M_*) < 10.5$ mass profile, which demonstrates a level of merging activity that is in tandem with the ‘All Galaxies’ profile peaking at $\sim 1.5 r_{200}$. These are clearly the two prominent subpopulations that drive the dynamic nature of the merging stack. The ‘All Galaxies’ profile shows a parity with the $\log_{10}(M_*) < 10.5$ profile throughout, suggesting the lower mass galaxies dominate the kinematics of the stack. At $\sim 1.5 r_{200}$ it appears there is a high level of mixed substructuring between the $\log_{10}(M_*) < 10.5$ and $\log_{10}(M_*) \geq 10.8$ populations. Where the ‘All Galaxies’ profile seems to indicate it is primarily composed of the two aforementioned subpopulations at larger radii. This is indicative of the occurrence of pre-processing by accretion of galaxies on to groups prior to cluster accretion. The intermediate profile of $10.5 \leq \log_{10}(M_*) < 10.8$ is the flattest, therefore, least dynamic of the populations within the stack.

The non-merging sample is comparatively dynamically relaxed with smaller dispersions and declining profiles that are not too dissimilar to the trend shown by Girardi et al. (1996). The $\log_{10}(M_*) < 10.5$ shows the closest parity with the ‘All Galaxies’ profile stack, again, suggesting low-mass galaxies dominate the kinematics. This profile possesses the highest dispersion of velocities within r_{200} , indicative of a young infalling population of galaxies. Whereas the $\log_{10}(M_*) \geq 10.8$ profile has the lowest dispersion within r_{200} . This

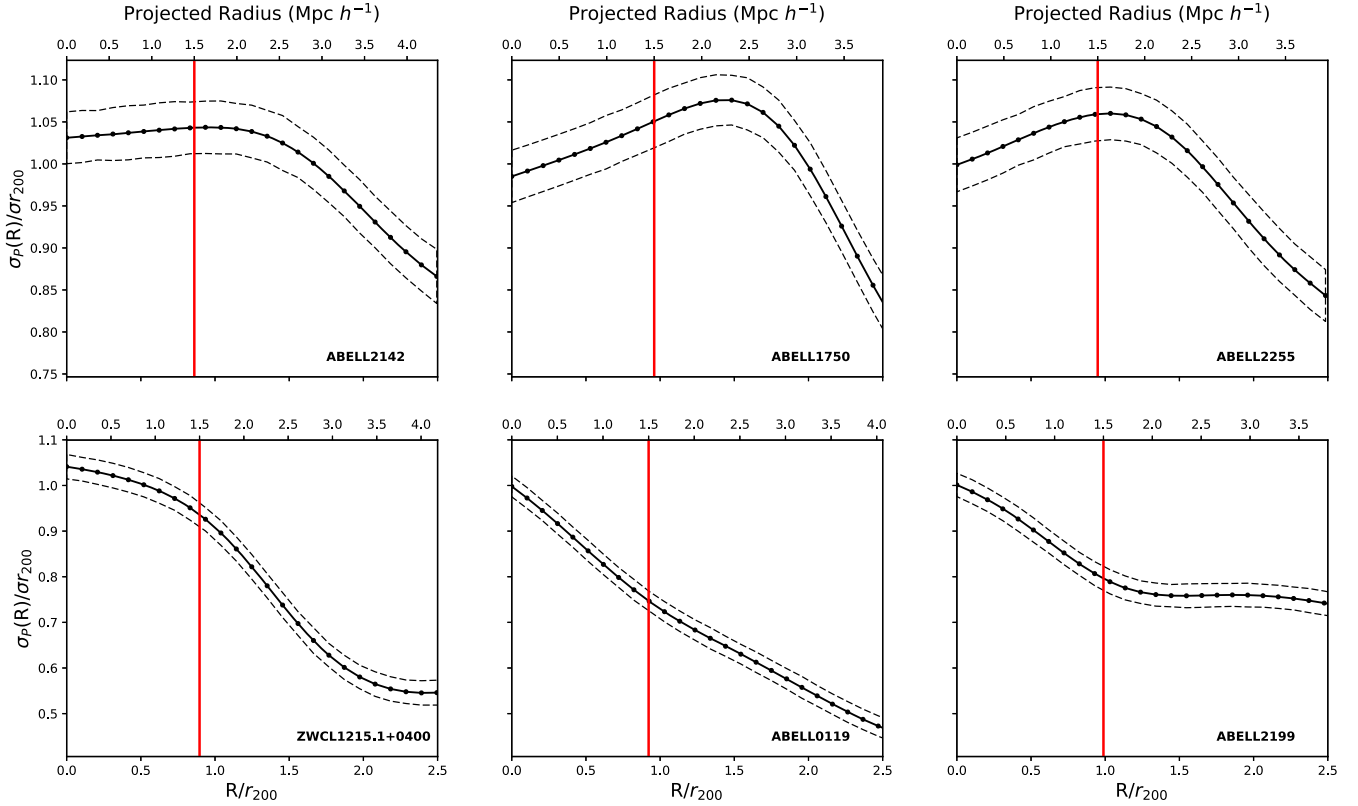


Figure 3. Example VDPs, consistent with those in Fig. 1, from the merging (top row) and non-merging (bottom row) subsamples plotted as a function of the projected virial radius r_{200} and normalized to their respective $\sigma_{r_{200}}$ values. The red vertical line indicates $1.5 \text{ Mpc } h^{-1}$ from the cluster centre where the global values and Δ test for substructuring are calculated. The dashed lines represent the 1σ uncertainty of 1000 monte carlo resamples. Note the rising profiles within $1.5 \text{ Mpc } h^{-1}$ in the merging clusters compared to the decreasing-to-flat profiles for the non-merging clusters within $1.5 \text{ Mpc } h^{-1}$.

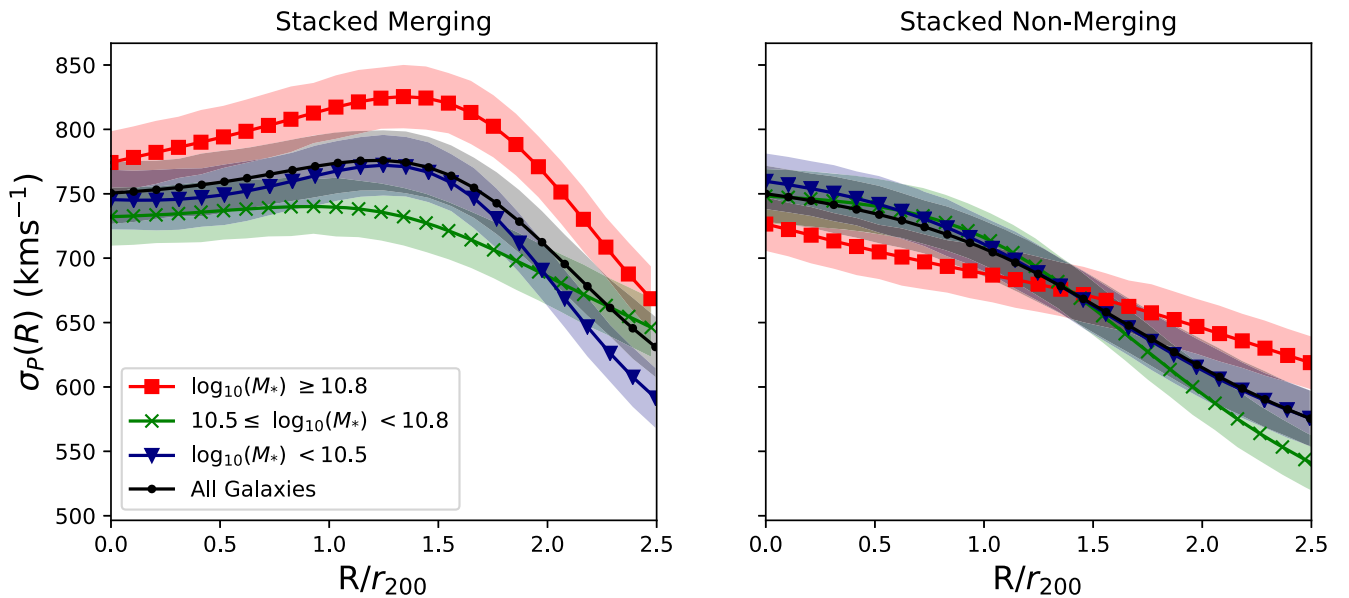


Figure 4. Co-added VDPs split by stellar mass for each cluster. Each profile represents a split by different intervals of $\log_{10}(M_*)$ as a function of radius (R/r_{200}), with the black profile representing all available galaxies within the sample. Shaded regions represent the 1σ uncertainty of 1000 monte carlo resamples.

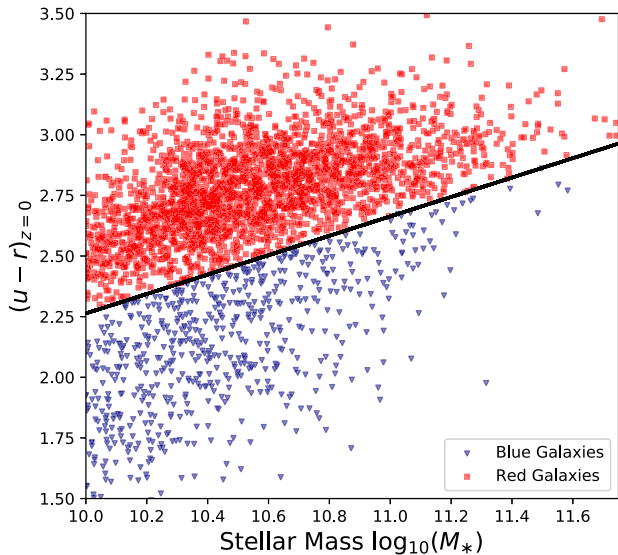


Figure 5. $(u - r)_{z=0}$ plotted as a function of $\log_{10}(M_*)$. The black line resembles the linear fit of the centre of the bimodal distribution at quartile increments of $\log_{10}(M_*)$; red galaxies are above the fitted line denoted as red squares; blue galaxies are below the fitted line denoted as blue triangles.

could be an indicator of an old population of galaxies slowly sloshing with the recently collapsed members on to cluster potentials. The $10.5 \leq \log_{10}(M_*) < 10.8$ profile blends in with the ‘All Galaxies’ and $\log_{10}(M_*) < 10.5$ profiles, suggesting there is little diversity between these populations of galaxies.

3.2 Colour

The cluster galaxies of each sample are passed through a colour limit gradient as a function of stellar mass. This is determined through the residuals of the bimodal distributions of colour in quartile increments of stellar mass (see Jin et al. 2014). This results in the

following linear relation

$$(u - r)_{z=0} = 0.40[\log_{10}(M_*)] - 1.74, \quad (4)$$

which as a consequence allows for an adequate boundary between red and blue galaxies that accounts for the biasing of galaxy colour distributions between low and high stellar masses. The resultant boundary line and the galaxy distributions can be seen in Fig. 5.

It should be noted that not all galaxies possess the used ‘modelMag’ DR8 photometry, therefore, some clusters experience a slightly reduced bin size compared to the principle MPA-JHU derived parameters. The galaxy colours are k -corrected to $z = 0$ prior to computing the VDPs with the imposed variable limit (see Chilingarian, Melchior & Zolotukhin 2010; Chilingarian & Zolotukhin 2012).

Fig. 6 depicts the merging sample to have a consistently high dispersion profile for the blue cloud stack at $\leq 1.5 r_{200}$, where the red sequence presents a shallow rising VDP with radius. However, there is a rising kinematic parity of the red sequence profile with the ‘All Galaxies’ profile throughout $\leq 1.5 r_{200}$. This behaviour could be an indicator the populations of blue, presumably star-forming, galaxies are kinematically active due to pre-processing of galaxies within the merging substructure with gradual infall on to the potential; Haines et al. (2015) highlight the need of pre-processing galaxies into groups to account for the level of quenching of star formation observed in cluster galaxies at large clustocentric radii. The rising profile of the red population with radius potentially demonstrates another environment of interacting galaxies, the profile leads to a rising VDP, indicating groupings of red galaxies at larger radii. These results evince a mixed population of merging blue galaxies alongside already pre-processed red galaxies in subgroupings at larger radii from the cluster centre.

The non-merging sample shows less dynamical variation, where all of the profiles present a shallow-to-flat variance with R/r_{200} . The shallow rising of the blue galaxy profile at $\sim 1.5 r_{200}$ could be an indicator of an infalling population of blue galaxies that have not tidally interacted with other clus-

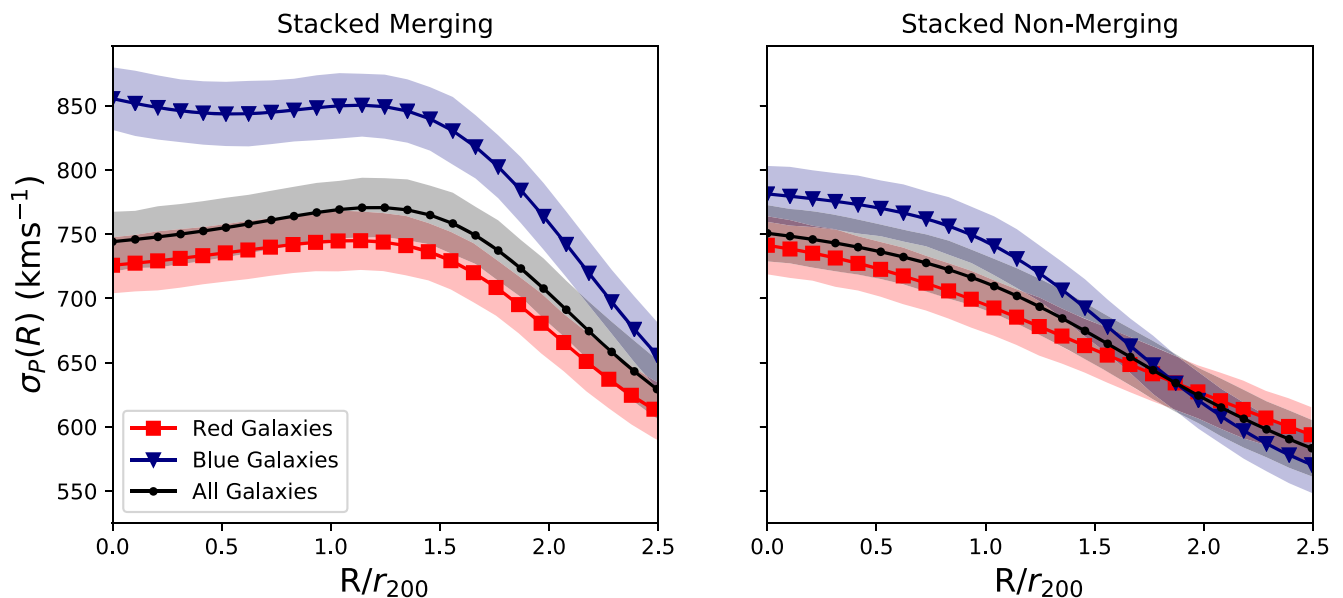


Figure 6. Stacked galaxy cluster VDPs split by their colour with the same axes as Fig. 4. Where the blue triangle and red square profiles represent the blue cloud and red sequence, respectively, with the black dot profiles representing all cluster galaxies available with colour data. Shaded regions represent the 1σ uncertainty of 1000 monte carlo resamples.

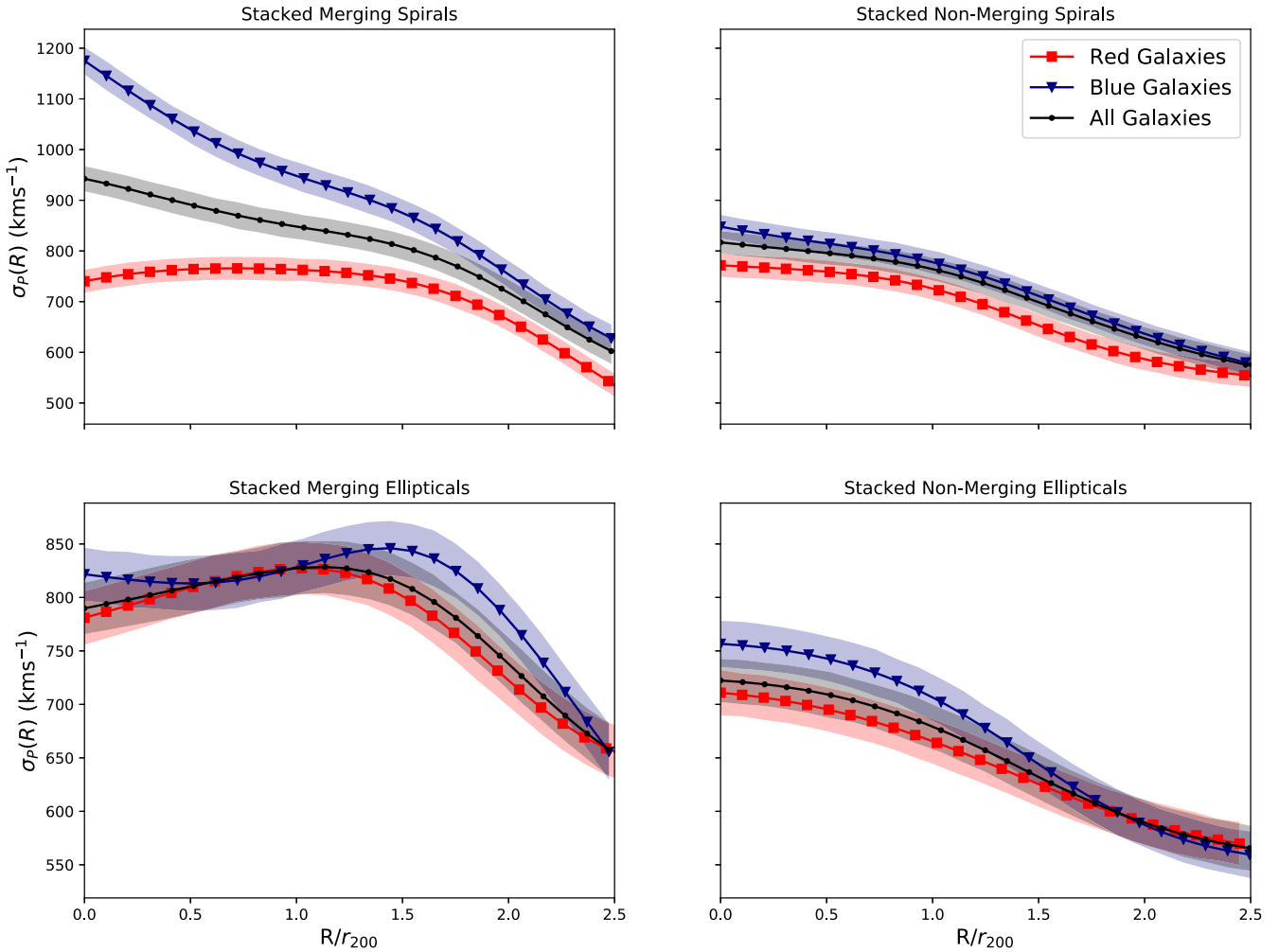


Figure 7. Co-added VDPs of spirals and ellipticals for each of the individual environments, which are then split by their bimodal colours as per Fig. 6. Shaded regions represent the 1σ uncertainty of 1000 monte carlo resamples.

ter members to the same degree as the merging counterpart. Comparatively, the red population profile presents gradual decrease from faster velocity dispersions at $\leq r_{200}$. There is the conspicuous observation of the merging red VDP in Fig. 4 representing high-mass galaxies in that it does not marry with what we would anticipate in comparison to the merging red VDP in Fig. 6 representing red galaxies. However, the mass limits in Section 3.1 are independent of colour, therefore, there is a mix of red and blue galaxies in the high-mass sample of galaxies. This is combined with a discrepancy in the sample sizes between a bimodal colour split and that of stellar mass which can be seen in Fig. 5, which is indicative that the red low-to-intermediate mass galaxies contribute to lower velocity dispersions. This behaviour does match with what Girardi et al. (1996) believe to indicate a neighbouring system or grouping of galaxies at larger radii. The direct comparison between the merging and non-merging samples in Fig. 6 demonstrates a more diverse variation of colour in dynamically relaxed clusters when compared to those that are dynamically complex, which has been discussed with recent observations made by Mulroy et al. (2017).

3.3 Morphology

The morphological classification of galaxies in clusters can be used as a proxy on how the local environment can lead to an alteration of their structure and shape. Therefore, utilizing the debiased morphological classification data of GZ2, this is married with the data of both merging and non-merging samples split by the same colour limits noted in Section 3.2. The samples are separated between umbrella spiral and elliptical morphologies, which is determined using the string classifier of 'gz2_class' by whether or not a galaxy possessed any number of spiral arms in its structure. It should be noted, however, that the relatively small number of galaxies classified within GZ2 ($\sim 300\,000$) means the average cluster membership can drop significantly. As a result the two clusters, Abell 0426 and Abell 0085, are not added to the stack for not meeting the richness criteria highlighted in Section 2. This drop in membership could lead to the average profiles being spurious due to the lack of a more complete data set. For each morphology in each environment, the cluster galaxies are then split into the same colours via the same linear relation as noted in Section 3.2.

Fig. 7 presents the resultant morphology–colour split. The merging spiral stack shows a declining blue population profile, which then converges with the ‘All Galaxies’ profile. This coincides with a near-flat profile of the spiral red population that starts to decline at $\sim r_{200}$. It is clear the merging spiral blue and red populations equally contribute to the total dispersion of merging spirals of the ‘All Galaxies’ VDP. However, there is a discrepancy from the conspicuously high dispersion of blue spiral galaxies within r_{200} , suggesting there is an infalling, or recently accreted, high-velocity population of blue spirals. The blue population profile of the merging ellipticals is fairly dynamic, leading to a bulk rise at $\sim 1.5 r_{200}$. This is indicative of a strongly interacting subpopulation of cluster galaxies, potentially as the result of tidal–tidal interactions through substructuring. The red elliptical profile, which shows a bulk rise at $\sim 1.2 r_{200}$, reaches close parity with the ‘All Galaxies’ profile, indicating the red ellipticals to be the main contributor to the ‘All Galaxies’ profile. The red ellipticals, like the blue ellipticals, present an interacting subpopulation within a merging environment; potentially these could be older pre-processed galaxies that were harassed into substructures at a subtly earlier epoch. The merging elliptical VDPs consist of mixed blue and red elliptical galaxies that have gone through pre-processing interactions beyond r_{200} . Both colour subpopulations in the merging elliptical stack are consistent with the blue and red merging subpopulations in Fig. 6, insinuating that ellipticals are the dominant contributors to a merging cluster environment.

In contrast with the non-merging sample, the spiral galaxies of both colour subpopulations steadily decline with radius. The non-merging ellipticals present a similar uniform of profiles that steadily decline with radius, aside from the slight increase in the dispersion of blue ellipticals at $\lesssim r_{200}$, suggesting they are recent members to collapse on to the cluster potential. The general slow decline observed with these non-merging profiles indicates a comparatively mixed ambient system of cluster galaxies. The merging VDPs are overtly dynamic, especially with the high dispersions in blue spiral cluster galaxies, or the variable profile shapes in the ellipticals, when compared to their non-merging counterparts. This is a clear indication of the differences in dynamical ages of the two environments; active feeding of a cluster potential through substructuring and infall compared to one that has reached a relaxed dynamical equilibrium.

4 DISCUSSION

The work presented here shows that across all intrinsic galactic parameter splits, the merging samples possess some form of rising profile. Hou et al. (2009) argue that such a rise indicates an interacting, or merging, system based on a correlation between a sample of non-Gaussian galaxy groups, coinciding with previous work by Menci & Fusco-Femiano (1996). However, these earlier works did not explicitly delineate which class(es) of galaxy are driving this.

4.1 Interpreting the VDPs

When analysing the ‘All Galaxies’ profiles for each split of the merging stacks, it can be deduced that these results seemingly back the argument made by Menci & Fusco-Femiano (1996) and Hou et al. (2009). With the non-merging samples generally showing a flat-to-declining series of profile. These results could corroborate recent work by Mulroy et al. (2017) that finds different cluster evolutionary histories must have played a part to explain the prominent colour variation observed in non-merging systems compared to that of merging systems. Deshev et al. (2017) are consistent with

this, observing a significant decrease in the fraction of star-forming galaxies in the core of the merging Abell 520 system compared against their non-merging sample, with evidence of a smaller group of galaxies, possessing a higher fraction of star-forming galaxies, feeding the merger. One explanation for this observation suggests a non-merging galaxy cluster is formed on long time-scales by their haloes inducing the infall, and accretion, through harassment of galaxies from the surrounding field population that leads to the gradual variation from red to blue colours with increasing radius from the centre seen in Mulroy et al. (2017). Whereas the merging systems are formed primarily from the accretion of pre-processed galaxy groups, meaning the galaxies have undergone heavy interactions leading to evolutionary changes, and are virialized to their local groupings.

We find the red populations of the merging stacks are the main contributors to the rising profiles, which illustrates a common and significant amount of interactions occurring at $\sim 1.5 r_{200}$ radii. Although, consideration should be taken into account that red galaxies could overshadow the total colour distribution of the cluster galaxy sample by numbers alone due to the Malmquist bias (Malmquist 1925), along with the making the sample complete, thereby impeding a true indication on how these two subpopulations behave kinematically. In comparison to the non-merging profiles that clearly illustrate a more relaxed environment with a possible suggestion of infalling blue galaxies, this married with the merging profiles showing the dominant driver of the rising profile shape to be a mix of red and blue elliptical subpopulations. The diverse dynamics between merging and non-merging systems provide further affirmation to the idea of a galaxy infall and accretion bimodality between merging and non-merging systems.

Considering the epochs of differing events that occur in a typical cluster (e.g. infall, accretion, splashback), we can use the time-scales between them to try and infer the current physical processes occurring and how they relate to their kinematics. Haines et al. (2015) simulate the accretion paths of multiple galaxies on to a massive cluster from various epochs and classify the infall regions to start $\lesssim 10 h^{-1}$ Mpc, or $\lesssim 5 r_{200}$. It is calculated that the time-scales from infall to accretion to be ~ 4 Gyr, a galaxy then becomes accreted once it reaches r_{200} and passes its first pericentre on time-scales of 0.5–0.8 Gyr, followed by a significantly slower of 2–3 Gyr for the galaxy to reach its first apocentre (splashback radius). Collectively, the VDPs demonstrate a period of infall in the merging stacks at $\leq r_{200}$, alongside a culmination of interactions occurring as a result of the domination of pre-processed groups. This is corroborated with the merging colour and morphology VDPs, where mixed blue and red populations of galaxies assumed to be undergoing pre-processing are infalling to be accreted on to the cluster, reaffirming the suggestion by Haines et al. (2015) that pre-processing is required to explain star formation being quenched at larger radii from the cluster centre. Furthermore, the VDPs representing spiral morphology could be indicating the galaxies at $\gtrsim 1.25 r_{200}$ are the start of an ~ 4 Gyr long journey on to the cluster potential, leading to their accretion and possible splashback, thus accounting for the larger surface density of spirals at smaller clustocentric radii (see Wetzel, Tinker & Conroy 2012; Haines et al. 2015; Cava et al. 2017).

In any case, there are increasingly more observations and simulations that appear to occasionally contradict, where many authors suggest a need for pre-processing (Haines et al. 2015; de Carvalho et al. 2017; Roberts & Parker 2017). Mulroy et al. (2017) argue for a bimodality on infall and accretion histories with similar accretion rates, one with pre-processing and one without, in order to explain the variations in colour found in non-merging systems.

Further simulations could possibly help to build on this picture for these bimodal, kinematic outcomes.

4.2 Phase-space caustics

In Section 2 we calculate velocity dispersions through a biweight method (Beers et al. 1990) and the phase-space surface caustics to determine cluster membership (Diaferio & Geller 1997; Diaferio 1999). The phase-space caustics produced from the chosen methodology follow a trumpet-shape pattern as we move away from the cluster centre, which is a result from galaxies infalling on to the cluster when the potential inundates the Hubble flow (Regos & Geller 1989). Diaferio & Geller (1997) and Diaferio (1999) both demonstrate the amplitudes of these surface caustics to be a product of random non-radial motions from substructuring, indicating a diverging caustic to be illustrative of a cluster with increasing interactions. Therefore, these caustics represent an escape velocity of the cluster potential. The key benefit, aside from powerfully indicating cluster boundaries, is that these caustics can be produced on redshift data alone. Unlike the rest of the literature, we allow the surface caustics to stretch to a ΔV velocity limit of $\pm 1500 \text{ km s}^{-1}$. This is to allow infallers to be added into the sample of cluster galaxies for each cluster, although, we wish to note that this method involves the risk of adding interloping larger scale structures to the sample. Many of the clusters compiled within this sample have been well studied, with calculated surface caustics and velocity dispersions. Reference values for the latter are presented in both Tables 1 and 2. The calculated $\sigma_{r_{200}}$ velocity dispersions are fairly consistent with the reference literature, however, there will be differences dependent on which method was used to estimate the velocity dispersions, at what radial point, and how many galaxies are available for the membership of the cluster at $\leq r_{200}$ in this work. What follows is a comparison of our phase-space surface caustic analysis with that of the literature.

4.2.1 Abell 85

Abell 85 is a well-studied cluster, with multiple calculations of its dispersion of velocities, along with phase-space surface caustics presented within Rines & Diaferio (2006). The value of $\sigma_{r_{200}}$ from this work is $\sim 200 \text{ km s}^{-1}$ offset from the calculated literature values. The primary driver of this offset is due their cluster membership being significantly greater with 497 galaxies within $1.7 r_{200}$ compared to 234 galaxies within $2.5 r_{200}$ from the data used here. The vast difference in galaxy membership can induce a slight alternate shape between the resultant surface caustics. Agulli et al. (2016) do not publish the surface caustics on their phase-space diagrams, leaving the surface caustics of Rines & Diaferio (2006), which indicate a strong constraint in ΔV -space at low radii. Despite the lack of sharp, sudden changes in the surface caustic with increasing R , there are still similarities in the membership from the caustic presented here against that of Rines & Diaferio (2006). This indicates there is consistency between the two independent calculations of the caustic surface that allows for a more liberal inclusion of galaxies into the membership.

4.2.2 Abell 119

Abell 119 possesses multiple surface caustics in the literature alongside calculations of their velocity dispersions (Rines et al. 2003; Rines & Diaferio 2006). There is, again, an offset of $\sim 100 \text{ km s}^{-1}$

in the calculation of $\sigma_{r_{200}}$, for which similar reasoning is applied from that of our discussion on Abell 85; the radial point at which the velocity dispersion is calculated can push the gaps between the literature further. Additionally, the techniques used for calculating the velocity dispersion from this work vary from that of Rines & Diaferio (2006), where sigma clipping is used (Zabludoff, Huchra & Geller 1990), this will lead to an underestimating of the velocity dispersion when directly compared to a biweight estimator. The phase-space caustics are the most consistent with the CAIRNS cluster study of Rines et al. (2003), with very similar profiles. These caustics only deviate where there are discrepancies in the number of galaxies within $\leq 10 \text{ Mpc } h^{-1}$. The recalculated caustics presented in Rines & Diaferio (2006) focus on constraining the cluster membership by limiting galaxies in ΔV -space to $\leq 1000 \text{ km s}^{-1}$, creating a surface caustic that is not as smooth, but is effective in the elimination of infallers and the encompassing large-scale structure.

4.2.3 Abell 426

Abell 426, commonly known as the ‘Perseus cluster’, does not presently possess any phase-space caustic analysis in the literature. Although, the phase-space surface caustics determined here are relatively simple, and the population of galaxies accumulated does not extend beyond $\sim 2 \text{ Mpc } h^{-1}$, providing a smooth distribution with several groupings of member galaxies. The limited and immediate break in the available data, due to the survey’s limitations in observing the north galactic cap, leads to an artificial increase in the VDP at larger radii. However, this affect should be reduced when stacked against the other clusters that extend beyond the projected radii of Abell 426. The velocity dispersions of Abell 426 determined within this work are not consistent with those determined within the literature, showing an offset of $\sim 500 \text{ km s}^{-1}$ (Struble & Rood 1999). The lack of consistency is a result of the significant loss of galaxy members compared to the true scale and size of Abell 426, which contains close to ~ 1000 galaxy members.

4.2.4 Abell 1650

Abell 1650 is an atypical cluster with a radio-quiet cD cluster galaxy at its centre. The surface caustics presented in the literature follow (Rines & Diaferio 2006) a similar shape and profile to our surface caustics, with a slight difference to the radial cut used on the sample of galaxies and a wider velocity window to allow for the addition of galaxy infallers. The velocity dispersions produced within this work are consistent with those of Einasto et al. (2012), within a slight discrepancy of $\sim 200 \text{ km s}^{-1}$. Although, the discrepancy in these values is expected due to differing methods used in calculating the dispersion.

4.2.5 Abell 1656

Abell 1656, commonly referred to as ‘Coma’, is a well-studied cluster with close to ~ 1000 members. It has such a strong presence within the literature primarily due to its relatively close proximity ($z \sim 0$), which results in a greater sacrifice of cluster galaxies when maintaining completeness. However, this is offset by the extremely high number density of cluster galaxies. The phase-space caustics of the coma cluster presented in this work are the most consistent with Sohn et al. (2017), this is the result of a more relaxed ΔV -space limit to accommodate the very large nature of the cluster. This consistency is lost at $\sim 4 \text{ Mpc } h^{-1}$ due to a sudden drop in galaxies

present within our MPA-JHU sample. However, an assumption can be made based the consistency is valid due to the trend of the caustic profile following that of Sohn et al. (2017) closely. The same consistency exists for the values of the velocity dispersion with very small offsets when compared to values from the literature (Rines et al. 2003; Sohn et al. 2017).

4.2.6 Abell 1750

Abell 1750 is a complex triple subcluster system in a pre-merger state, which is briefly discussed in Section 4.3. The phase-space surface caustics presented here are the most consistent with produced by Rines & Diaferio (2006), with the exception of allowing infallers at $\sim 2 \text{ Mpc } h^{-1}$ to form the cluster membership. The literary values of the velocity dispersion show a discrepancy of $\sim 100 \text{ km s}^{-1}$ from the values calculated in this work (Rines & Diaferio 2006; Einasto et al. 2012). What does remain consistent is the reasoning that alternative, less robust, methods were used to calculate a value for σ . As well as this, there is a lack of clarity on the exact methodology used to calculate the dispersions of velocities within some of the literature where alternative limits could have been used within their calculations that are otherwise unstated.

4.2.7 Abell 1795

Abell 1795 is a cool core galaxy cluster with an unusually large cavity with no counterpart (Walker, Fabian & Kosec 2014). There is currently no phase-space surface caustic analysis within the literature that can be aided to check consistency. However, from our own determined caustics we can see there is a roughly even distribution of member galaxies close to the centre of the cluster, as expected from a typical relaxed cluster. Our calculated velocity dispersion is consistent with those values found in the literature (Zhang et al. 2011; Einasto et al. 2012).

4.2.8 Abell 2029

Abell 2029 is a massive cluster that possesses a powerful cD galaxy at its centre, forming part of a supercluster with complex dynamical interactions within the ICM (Walker et al. 2012). Sohn et al. (2017) have produced surface caustics of Abell 2029 that are inconsistent with our own. There are gaps in the galaxy population size within the phase-space diagram due to the redshift limitations of the MPA-JHU DR8 data. These limitations make our data incomplete for this cluster, whereas Sohn et al. (2017) have used complementary sets of data, and therefore, do not possess the same restrictions as those found in this work. However, the bulk of the galaxies present within the imposed limits of this work match those defined as members within the phase-space surface caustic diagrams of Sohn et al. (2017) that include infallers. The velocity dispersion calculated in this work is consistent with other determined values within the literature despite the variances in galaxy membership.

4.2.9 Abell 2061

Abell 2061 is a double subcluster system with complex dynamics that is in close proximity to Abell 2067; this is highlighted in more detail in Section 4.3. The comprehensive CIRS survey by Rines & Diaferio (2006) presents consistent phase-space surface caustics when in consideration for the discrepancy in the range of velocities

used. The only discrepancy of note is the presence of strong foreground substructuring at $\sim 3.5 \text{ Mpc } h^{-1}$ inducing the caustic profile to maintain a consistent velocity of $\sim 1000 \text{ km s}^{-1}$, which causes the VDP to slightly increase beyond the σ_{r200} values. The literary values for Abell 2061's velocity dispersion are consistent with our own where Pearson et al. (2014) present an offset of $\sim 100 \text{ km s}^{-1}$, however, this is primarily due to the tighter distribution of galaxies, as well as differing methodologies for calculating the dispersion.

4.2.10 Abell 2065

Abell 2065, at present, does not have any detailed phase-space analysis within the literature for direct comparison. However, from our own analysis, Abell 2065 possesses what appears to be a strong bimodal distribution, which can be attributed to a complex dynamical system of multiple substructures. This would provide consistency, since Abell 2065 is stated in the literature to possess an unequal core merger, for which the full nature of this is detailed in Section 4.3. We believe the relatively flat velocity offset at $\sim -2000 \text{ km s}^{-1}$ with increasing R to be the smaller of the two cores. The state of initial merger makes it difficult for the surface caustics to discern where the cluster ends and begins. However, the string of flat galaxies implies something akin to the Kaiser effect (Kaiser 1987), where a flat radial separation against a non-flat separation in the plane of the sky leads to the inference of infallers.

4.2.11 Abell 2142

Abell 2142 is a notorious cluster for its smooth and symmetric X-ray emission, indicative of a post-core-merger event, which occurred ~ 1 billion years ago (Markevitch et al. 2000). The phase-space surface caustics of Abell 2142 vary within the literature, as well as in comparison to the work done here. Munari et al. (2014) present surface caustics within the confines of $\sim 3 \text{ Mpc } h^{-1}$ and appear to be constant with increasing R . Again, with Rines & Diaferio (2006) demonstrating a more dynamic and tighter caustic due to differing limits applied in both velocity-space and radial-space alongside data visualization effects. As usual, the shapes of these caustics are determined by the numbers of galaxies present within the field and how closely, or sparsely, they are distributed as we increase R from the cluster centre. Again, the calculated velocity dispersions from Munari et al. (2014) are inconsistent with our own value, offset by $\sim 300 \text{ km s}^{-1}$. This is due to the spread, number, and density of the cluster membership determined in the work of Munari et al. (2014) being equally greater.

4.2.12 Abell 2199

Abell 2199 is a relatively local galaxy cluster and provides a good testing bed for large-scale structure formation thanks to its close proximity, this is akin to Abell 1656, another relatively local cluster. The cluster is well studied, possessing several phase-space surface caustics in the literature. The phase-space caustics in this work are the most consistent with Song et al. (2017) and Rines et al. (2003), where the shape and profile closely match despite a lower membership. The velocity dispersions calculated here are consistent with those found within the literature (Rines et al. 2003).

4.2.13 Abell 2255

Abell 2255 is a merging galaxy cluster with a complex X-ray distribution, which has yielded a variety of studies to better understand the mechanisms of diffuse radio emission (Akamatsu et al. 2017). The total membership of Abell 2255 in this work is considerably less than that of other literature. However, the surface caustics of this work are still reasonably consistent with the caustics determined by Rines & Diaferio (2006), if lacking in definition. The VDPs determined here are consistent with those in the literature, despite offsets of $\sim 200 \text{ km s}^{-1}$, the drivers are variations in galaxy membership (Zhang et al. 2011; Akamatsu et al. 2017).

4.2.14 ZWCL1215

The phase-space caustics of galaxy cluster ZWCL1215 determined in this body of work are consistent with those that are produced by Rines & Diaferio (2006), with only slight variations in the definition of the shape of the surface caustics. The calculated velocity dispersions are also consistent with those determined by Zhang et al. (2011), with an offset of $\sim 200 \text{ km s}^{-1}$, as a result of the reduced membership of galaxies presented within this work.

4.3 Interloping structures

The clusters that form our sample are not purely isolated potentials, therefore we should take into consideration potential interloping structures as a result of a cluster being a member of supercluster. As an example, during the data accumulation stage of Section 2, the clusters are cross-matched against the Einasto et al. (2001) catalogue of superclusters to determine any significant contamination between clusters. Abell 2244 and Abell 2249 are eliminated from the samples due to their strong interloping/overlap in RA–DEC space and z -space within the regions being investigated within this work. Although, their removal from the samples has not altered the shape of the final stacked VDPs to any significant degree.

There are also other clusters within the sample that possess unusual substructures. The phase-space diagram of Abell 2065 in Fig. 1 clearly presents two seemingly independent structures. However, Abell 2065 has been documented in the literature to be at the late stage of an ongoing merger (Markevitch, Sarazin & Vikhlinin 1999). Further X-ray observations with *XMM-Newton* indicate more specifically the presence of an ongoing compact merger between two subclusters within Abell 2065, where the two cores are at an epoch of initial interaction (Belsole et al. 2005). Higher resolution X-ray observations from *Chandra* show a surviving cool core from the initial merger, with an upper limit merger velocity of $\lesssim 1900 \text{ km s}^{-1}$, adding to the argument that Abell 2065 is an unequal core merger (see Chatzikos, Sarazin & Kempner 2006). This provides an explanation to the slightly off-centre line-of-sight mean velocity distribution of galaxies, with a second, smaller core averaging out to $\sim -1500 \text{ km s}^{-1}$ found in the phase-space diagram of Abell 2065, and naturally will affect the shape of the VDP at larger radii. Abell 1750 is a triple subcluster system with the north subcluster separated from the central subcluster by a velocity offset of -900 km s^{-1} and are all currently in a stage of pre-merger to the point where the plasma between the substructures is significantly perturbed (Molnar et al. 2013; Bulbul et al. 2016). In contrast Abell 2061, which resides within the gravitationally bound Corona Borealis supercluster with Abell 2065 (see Pearson et al. 2014), possesses two optical substructures that will affect the VDP similarly to Abell 2061 (van Weeren et al. 2011). It should be noted

that Abell 2061 potentially forms a bound system with the smaller cluster/group Abell 2067 (Marini et al. 2004; Rines & Diaferio 2006), with line-of-sight velocity separation of $\sim 725 \text{ km s}^{-1}$ (Abdullah et al. 2011). Observations hint at a likely filament connecting the two systems (Farnsworth et al. 2013) aiding to the suggestion of cluster–cluster interloping. There is ~ 30 arcmin of sky separation and with the prescribed cosmology in Section 1 this provides a rough projected distance of $\sim 2.7 \text{ Mpc } h^{-1}$ from the centre of Abell 2061. Yet, this confirms to the cluster–cluster overlapping suggestion with the criteria used to develop cluster membership. Therefore, it is very likely the membership of Abell 2061 is contaminated with the infalling Abell 2067 cluster’s member galaxies as we approach $2.5 R/r_{200}$.

4.4 The delta test

The process of determining whether or not a cluster is merging involved the use of the Δ test for substructure, devised by Dressler & Shectman (1988). Whereby the presence of any substructure to a ≥ 99 per cent significance is recorded as a merging cluster environment. The Δ test, while a powerful and sensitive tool, is limited in its power to test for substructure since it only concerns itself with the sum of the deviations of a local velocity dispersion and mean recession velocity with global cluster values. This could lead to a greater probability of false positives for substructuring, along with omissions of those clusters that genuinely possess it. The problem becomes more apparent if an appropriate radial cut-off is not applied when calculating Δ , otherwise the test will classify nearly every cluster to contain substructure. This is a consequence of the varying numbers of cluster galaxies that are added into the calculation of Δ ; greater numbers of cluster galaxies help decrease the value of $P(\Delta)$, thereby artificially increasing the significance of subclustering and vice versa. Pinkney et al. (1996) highlight in their comparison of substructure tests how the sensitivity of the Δ test is affected measurably by the projection angle of the member galaxies; this can lead to a potential loss of genuine merging systems from our subsample when their velocities run along 0° or 90° . One way to potentially alleviate this could be the introduction of more spatial parameters. For example, the *Lee Three-Dimensional Statistic* adapted by Fitchett & Webster (1987) took into consideration angles derived from the projected space and velocity. This test can help to eliminate any potential false positive with its ability to be insensitive to genuine non-merging systems (Pinkney et al. 1996).

There are also methods for testing dynamical activity that involve measuring the Gaussianity of the velocity distributions, such as the ‘Hellinger Distance’ measuring the distance between a set of observational and theoretical distributions (see Ribeiro et al. 2013; de Carvalho et al. 2017). Other novel approaches, such as one presented by Schwinn et al. (2018), test to see whether 2D mass maps can be used to find mass peaks using wavelet transform coefficients, highlighting discrepancies between definitions of substructure. In contrast, tried and tested methods are evaluated by Hou et al. (2009), comparing different approaches to analysing the dynamical complexity to groups of galaxies. The authors find a χ^2 goodness-of-fit is not best suited for determining a transition away from a Gaussian distribution of velocities. The principle upon which the Δ test is built upon is a frequentist χ^2 , which may indicate there is some form of decoupling in the link between substructuring and dynamical activity. This apparent decoupling is most likely a result of the limitations of using a singular technique to define if a merging

system of cluster galaxies is present, as the Δ test is only sensitive to average deviations from observed line-of-sight velocities. This is a problem that extends to the VDPs, since they rely on a weighted grouping of objects in velocity-space with a moving Gaussian window function. Therefore, care has to be taken when classifying a galaxy cluster as merging or non-merging based on using the methodology of Bergond et al. (2006) and Hou et al. (2009). Despite these caveats, the nature of determining substructure with classical statistical testing is simple, sensitive and allows for fast computation on determining our subsamples. However, there is room to consider how one can accurately define a cluster to be merging or not based solely on limiting velocity-space tests for substructure/grouping of galaxies. For example, there are relic mergers with non-thermal emissions that represent an afterglow of a merging event, or, represent a pre-merging environment as a result from the interactions between intracluster media (e.g. Giovannini et al. 2009; Bulbul et al. 2016). These environments would be insensitive to our traditional statistical testing for substructure due to its constrained application on using the clustering of galaxies as the sole proxy for a merging system. Utilizing other parts of the spectrum highlights strong interactions between particles of the ICM, or, of two interacting ICMs from two initially independent systems, and the lack of a comprehensive study can call into question how we best define what is and is not a merging cluster.

The VDPs produced here could potentially mask any further variability within the kinematics that would otherwise be visible on a smaller scale ‘window width’. It is apparent from this work there is some form of sublayer to the profiles that inhibit a clearer picture being formed in the dynamical nature of galaxies with differing properties. It is a notable possibility that, within some clusters, there is still an inclusion of interloper field galaxies towards $\sim 2.5 r_{200}$ that distort our final view on the key drivers of these seemingly interacting galaxy subpopulations. The differing merging and non-merging sample sizes present problems of their own that lead to biasing the final stacked VDPs. For example, the smoothing kernel, along with the chosen width of the kernel, used will cause a decrease in the sensitivity in how the VDPs respond to substructuring. This problem continues with the stacking procedures, which decrease the sensitivity to the presence of mergers due to each cluster possessing unique environments with different position angles and separations. This problem is further extended when clusters possess limited numbers due to spectroscopic limitations of the survey in the MPA-JHU data. Therefore, unless there is a significant number of galaxies inputted to the calculation of a VDP, the risk of spurious features appearing is still a powerful one. In some cases this is purely a limitation of the data available from marrying the MPA-JHU with DR8 photometry or GZ2 morphologies, in others, an indicator of the limitations in using VDPs as a tool to present the dynamical overview of galaxy clusters.

5 SUMMARY

In this work we have produced a base line cluster galaxy membership that marries the MPA-JHU DR8 archival data with the BAX limits of $(3 < L_X < 30) \times 10^{44} \text{ erg s}^{-1}$ and $0.0 < z < 0.1$, which is complete at $\log_{10}(M_*) > 10.1$. The sample of galaxy clusters is sub-categorized into merging or non-merging samples of galaxy clusters depending on the outcome of the Dressler & Shectman (1988) test. Stacks of VDPs are computed for differing galactic parameters in order to determine what drives the shape of the VDP.

The key results are summarized as follows:

- (i) In common with previous literature, our merging cluster sample demonstrates a steeply rising VDP. The bulk of this rise happens at $\sim 1.5 r_{200}$. On the other hand, non-merging clusters generally exhibit a declining-to-flat VDP.
- (ii) In merging systems, a mix of red and blue elliptical galaxies appear to be driving the rising VDP at these radii. This may be the result of pre-processing within galaxy groups.
- (iii) Non-merging systems commonly display little variation in kinematics throughout their VDPs, however, there are consistently higher $\sigma_p(R)$ values from the VDPs associated with a younger population of galaxies.
- (iv) Spiral galaxy VDPs in merging systems present a dichotomy in their dispersion of velocities, with the blue spiral galaxies possessing a high velocity dispersion that is indicative of an infalling subpopulation of field galaxies.
- (v) The global VDP of an individual cluster must be treated with care since a rising or falling VDP may be driven by a subpopulation of the cluster members.

ACKNOWLEDGEMENTS

We extend our thanks to the referees for their valued time in offering thorough feedback and suggestions to this work, providing a valuable second opinion.

We would like to thank Bill Harris for his assistance and advice with regard to the Gaussian smoothing kernel used within this work.

LEB wishes to thank Yjan Gordon for his continued help and advice throughout the formulation of this work.

We acknowledge the support of STFC through the University of Hull’s Consolidated Grant ST/R000840/1.

This research made use of Astropy, a community-developed core Python package for Astronomy (Astropy Collaboration 2013; The Astropy Collaboration 2018).

This research has made use of the X-Rays Clusters Database (BAX) that is operated by the Laboratoire d’Astrophysique de Tarbes-Toulouse (LATT), under contract with the Centre National d’Etudes Spatiales (CNES).

This research has made use of the ‘K-corrections calculator’ service available at <http://kcor.sai.msu.ru/>.

Funding for SDSS-III has been provided by the Alfred P. Sloan Foundation, the Participating Institutions, the National Science Foundation, and the U.S. Department of Energy Office of Science. The SDSS-III website is <http://www.sdss3.org/>. SDSS-III is managed by the Astrophysical Research Consortium for the Participating Institutions of the SDSS-III Collaboration including the University of Arizona, the Brazilian Participation Group, Brookhaven National Laboratory, Carnegie Mellon University, University of Florida, the French Participation Group, the German Participation Group, Harvard University, the Instituto de Astrofísica de Canarias, the Michigan State/Notre Dame/JINA Participation Group, Johns Hopkins University, Lawrence Berkeley National Laboratory, Max Planck Institute for Astrophysics, Max Planck Institute for Extraterrestrial Physics, New Mexico State University, New York University, Ohio State University, Pennsylvania State University, University of Portsmouth, Princeton University, the Spanish Participation Group, University of Tokyo, University of Utah, Vanderbilt University, University of Virginia, University of Washington, and Yale University.

REFERENCES

- Abadi M. G., Moore B., Bower R. G., 1999, *MNRAS*, 308, 947
- Abdullah M. H., Ali G. B., Ismail H. A., Rassem M. A., 2011, *MNRAS*, 416, 2027
- Agulli I., Aguerri J. A. L., Sánchez-Janssen R., Dalla Vecchia C., Diaferio A., Barrena R., Dominguez Palmero L., Yu H., 2016, *MNRAS*, 458, 1590
- Aihara H. et al., 2011, *ApJS*, 193, 29
- Akamatsu H. et al., 2017, *A&A*, 600, A100
- Bahé Y. M., McCarthy I. G., Balogh M. L., Font A. S., 2013, *MNRAS*, 430, 3017
- Balogh M. L., Morris S. L., Yee H. K. C., Carlberg R. G., Ellingson E., 1999, *ApJ*, 527, 54
- Bamford S. P. et al., 2009, *MNRAS*, 393, 1324
- Baxter E. et al., 2017, *ApJ*, 841, 18
- Beers T. C., Flynn K., Gebhardt K., 1990, *AJ*, 100, 32
- Belsole E., Sauvageot J.-L., Pratt G. W., Bourdin H., 2005, *Adv. Space Res.*, 36, 630
- Bergond G., Zepf S. E., Romanowsky A. J., Sharples R. M., Rhode K. L., 2006, *A&A*, 448, 155
- Berrier J. C., Stewart K. R., Bullock J. S., Purcell C. W., Barton E. J., Wechsler R. H., 2009, *ApJ*, 690, 1292
- Blanton M. R., Lupton R. H., Schlegel D. J., Strauss M. A., Brinkmann J., Fukugita M., Loveday J., 2005, *ApJ*, 631, 208
- Böhringer H. et al., 2000, *ApJS*, 129, 435
- Brinchmann J., Charlot S., White S. D. M., Tremonti C., Kauffmann G., Heckman T., Brinkmann J., 2004, *MNRAS*, 351, 1151
- Bulbul E. et al., 2016, *ApJ*, 818, 131
- Cava A. et al., 2017, *A&A*, 606, A108
- Chatzikos M., Sarazin C. L., Kempner J. C., 2006, *ApJ*, 643, 751
- Chilingarian I. V., Zolotukhin I. Y., 2012, *MNRAS*, 419, 1727
- Chilingarian I. V., Melchior A.-L., Zolotukhin I. Y., 2010, *MNRAS*, 405, 1409
- Astropy Collaboration, 2013, *A&A*, 558, A33
- The Astropy Collaboration, 2018, *AJ*, 156, 123
- Cortese L. et al., 2007, *MNRAS*, 376, 157
- Danese L., de Zotti G., di Tullio G., 1980, *A&A*, 82, 322
- de Carvalho R. R., Ribeiro A. L. B., Stalder D. H., Rosa R. R., Costa A. P., Moura T. C., 2017, *AJ*, 154, 96
- Deshev B. et al., 2017, *A&A*, 607, A131
- Diaferio A., 1999, *MNRAS*, 309, 610
- Diaferio A., Geller M. J., 1997, *ApJ*, 481, 633
- Dressler A., 1980, *ApJ*, 236, 351
- Dressler A., Shectman S. A., 1988, *AJ*, 95, 985
- Einasto M., Einasto J., Tago E., Müller V., Andernach H., 2001, *AJ*, 122, 2222
- Einasto M. et al., 2012, *A&A*, 540, A123
- Farnsworth D., Rudnick L., Brown S., Brunetti G., 2013, *ApJ*, 779, 189
- Fitchett M., Webster R., 1987, *ApJ*, 317, 653
- Freng C. S. et al., 1999, *ApJ*, 525, 554
- Gavazzi G., Boselli A., Mayer L., Iglesias-Paramo J., Vílchez J. M., Carrasco L., 2001, *ApJ*, 563, L23
- Gifford D., Miller C. J., 2013, *ApJ*, 768, L32
- Gifford D., Miller C., Kern N., 2013, *ApJ*, 773, 116
- Giovannini G., Bonafede A., Feretti L., Govoni F., Murgia M., Ferrari F., Monti G., 2009, *A&A*, 507, 1257
- Girardi M., Fadda D., Giuricin G., Mardirossian F., Mezzetti M., Biviano A., 1996, *ApJ*, 457, 61
- Gómez P. L. et al., 2003, *ApJ*, 584, 210
- Gunn J. E., Gott J. R., III, 1972, *ApJ*, 176, 1
- Haines C. P. et al., 2009, *ApJ*, 704, 126
- Haines C. P. et al., 2015, *ApJ*, 806, 101
- Hart R. E. et al., 2016, *MNRAS*, 461, 3663
- Hogg D. W. et al., 2003, *ApJ*, 585, L5
- Hogg D. W. et al., 2004, *ApJ*, 601, L29
- Hou A., Parker L. C., Harris W. E., Wilman D. J., 2009, *ApJ*, 702, 1199
- Hou A. et al., 2012, *MNRAS*, 421, 3594
- Jin S.-W., Gu Q., Huang S., Shi Y., Feng L.-L., 2014, *ApJ*, 787, 63
- Kaiser N., 1987, *MNRAS*, 227, 1
- Kauffmann G. et al., 2003, *MNRAS*, 341, 33
- Kauffmann G., White S. D. M., Heckman T. M., Ménard B., Brinchmann J., Charlot S., Tremonti C., Brinkmann J., 2004, *MNRAS*, 353, 713
- Larson R. B., Tinsley B. M., Caldwell C. N., 1980, *ApJ*, 237, 692
- Lewis I. et al., 2002, *MNRAS*, 334, 673
- Malmquist K. G., 1925, *Meddelanden fran Lunds Astronomiska Observatorium Serie I*, 106, 1
- Marini F. et al., 2004, *MNRAS*, 353, 1219
- Markevitch M., Sarazin C. L., Vikhlinin A., 1999, *ApJ*, 521, 526
- Markevitch M. et al., 2000, *ApJ*, 541, 542
- Markevitch M., Gonzalez A. H., David L., Vikhlinin A., Murray S., Forman W., Jones C., Tucker W., 2002, *ApJ*, 567, L27
- Menci N., Fusco-Femiano R., 1996, *ApJ*, 472, 46
- Molnar S. M., Chiu I.-N. T., Broadhurst T., Stadel J. G., 2013, *ApJ*, 779, 63
- Moore B., Katz N., Lake G., Dressler A., Oemler A., 1996, *Nature*, 379, 613
- Moore B., Lake G., Quinn T., Stadel J., 1999, *MNRAS*, 304, 465
- More S., Diemer B., Kravtsov A. V., 2015, *ApJ*, 810, 36
- More S. et al., 2016, *ApJ*, 825, 39
- Mulroy S. L., McGee S. L., Gillman S., Smith G. P., Haines C. P., Démoclès J., Okabe N., Egami E., 2017, *MNRAS*, 472, 3246
- Munari E., Biviano A., Mamon G. A., 2014, *A&A*, 566, A68
- Oemler A., Jr, 1974, *ApJ*, 194, 1
- Owers M. S., Randall S. W., Nulsen P. E. J., Couch W. J., David L. P., Kempner J. C., 2011, *ApJ*, 728, 27
- Owers M. S., Couch W. J., Nulsen P. E. J., Randall S. W., 2012, *ApJ*, 750, L23
- Pearson D. W., Batiste M., Batuski D. J., 2014, *MNRAS*, 441, 1601
- Pimblet K. A., Jensen P. C., 2012, *MNRAS*, 426, 1632
- Pimblet K. A., Smail I., Edge A. C., O'Hely E., Couch W. J., Zabludoff A. I., 2006, *MNRAS*, 366, 645
- Pimblet K. A., Penny S. J., Davies R. L., 2014, *MNRAS*, 438, 3049
- Pinkney J., Roettiger K., Burns J. O., Bird C. M., 1996, *ApJS*, 104, 1
- Popesso P., Biviano A., Böhringer H., Romaniello M., 2007, *A&A*, 461, 397
- Postman M., Geller M. J., 1984, *ApJ*, 281, 95
- Quilis V., Moore B., Bower R., 2000, *Science*, 288, 1617
- Regos E., Geller M. J., 1989, *AJ*, 98, 755
- Reiprich T. H., Böhringer H., 2002, *ApJ*, 567, 716
- Ribeiro A. L. B., de Carvalho R. R., Trevisan M., Capelato H. V., La Barbera F., Lopes P. A. A., Schilling A. C., 2013, *MNRAS*, 434, 784
- Rines K., Diaferio A., 2006, *AJ*, 132, 1275
- Rines K., Geller M. J., Kurtz M. J., Diaferio A., 2003, *AJ*, 126, 2152
- Roberts I. D., Parker L. C., 2017, *MNRAS*, 467, 3268
- Roediger E., Brüggem M., 2007, *MNRAS*, 380, 1399
- Sadat R., Blanchard A., Kneib J.-P., Mathez G., Madore B., Mazzarella J. M., 2004, *A&A*, 424, 1097
- Sanchis T., Mamon G. A., Salvador-Solé E., Solanes J. M., 2004, *A&A*, 418, 393
- Schwinn J., Baugh C. M., Jauzac M., Bartelmann M., Eckert D., 2018, preprint ([arXiv:1804.07401](https://arxiv.org/abs/1804.07401))
- Sheen Y.-K. et al., 2017, *ApJ*, 840, L7
- Smith G. P., Treu T., Ellis R. S., Moran S. M., Dressler A., 2005, *ApJ*, 620, 78
- Sohn J., Geller M. J., Zahid H. J., Fabricant D. G., Diaferio A., Rines K. J., 2017, *ApJS*, 229, 20
- Song H., Hwang H. S., Park C., Tamura T., 2017, *ApJ*, 842, 88
- Struble M. F., Rood H. J., 1999, *ApJS*, 125, 35
- Tremonti C. A. et al., 2004, *ApJ*, 613, 898
- Tucker W. et al., 1998, *ApJ*, 496, L5
- van Weeren R. J., Brüggem M., Rottgering H. J. A., Hoeft M., Nuza S. E., Intema H. T., 2011, *A&A*, 533, A35
- von der Linden A., Wild V., Kauffmann G., White S. D. M., Weinmann S., 2010, *MNRAS*, 404, 1231
- Walker S. A., Fabian A. C., Sanders J. S., George M. R., Tawara Y., 2012, *MNRAS*, 422, 3503
- Walker S. A., Fabian A. C., Kosec P., 2014, *MNRAS*, 445, 3444

Wetzel A. R., Tinker J. L., Conroy C., 2012, *MNRAS*, 424, 232

Willett K. W. et al., 2013, *MNRAS*, 435, 2835

Woodley K. A., Harris W. E., Beasley M. A., Peng E. W., Bridges T. J.,
Forbes D. A., Harris G. L. H., 2007, *AJ*, 134, 494

Wright E. L., 2006, *PASP*, 118, 1711

Zabludoff A. I., Huchra J. P., Geller M. J., 1990, *ApJS*, 74, 1

Zhang Y.-Y., Andernach H., Caretta C. A., Reiprich T. H., Böhringer H.,
Puchwein E., Sijacki D., Girardi M., 2011, *A&A*, 526, A105

This paper has been typeset from a $\text{\TeX}/\text{\LaTeX}$ file prepared by the author.